Journal of Materials Science: Materials in Electronics (2020) 31:6530–6537
https://doi.org/10.1007/s10854-020-03209-w

Electrooxidation behavior of ethanol toward carbon microbead-encapsulated ZnO particles derived from coffee waste

Zafar Khan Ghouri[1] · Khaled Elsaid[1] · Ahmed Abdel-Wahab[1] · Ahmed Abdala[1] · Mohammad Zahid Farhad[2]

Received: 15 December 2019 / Accepted: 4 March 2020 / Published online: 18 March 2020

Abstract
Carbon microbead-encapsulated ZnO (CM-ZnO) particles have been synthesized from the spent coffee ground (SCG) by chemical activation with $ZnCl_2$ followed by calcination at 700 ℃ in N_2 environment. Interestingly, $ZnCl_2$ can act as an activating agent as well as a precursor for ZnO particles. The structure of the core and shell of the CM-ZnO was investigated by scanning electron microscopy (SEM) and transmission electron microscopy (TEM) techniques. Moreover, X-ray diffraction (XRD) and energy-dispersive spectroscopy (EDS) studies confirmed the presence of the encapsulated ZnO particles. The Brunauer–Emmett–Teller (BET) and Barrett–Joyner–Halenda (BJH) plots showed a well-developed porous structure with a specific surface area of 210 m^2/g, average pore volume of 1.12 cm^3/g, and an average pore radius of 31.7 Å. The electrooxidation behavior of ethanol toward the synthesized CM-ZnO was then studied using cyclic voltammetry (CV) technique. For comparison, two types of modified electrodes were prepared: the first one with the non-activated SCG and the second one with the CM-ZnO. The electrochemical measurements of the prepared CM-ZnO demonstrated higher electrocatalytic activity with a current density of ~ 35 mA/cm^2 at 0.4 V vs. Ag/AgCl for ethanol electrooxidation in an alkaline medium. The electrochemical measurements specified that the presence of ZnO particles and the high surface area of the activated sample have a significant influence on electrooxidation activity. Therefore, the introduced CM-ZnO particles could be an alternative and effective non-precious electrocatalyst for ethanol electrooxidation.

1 Introduction

The world is expected to face an undeniable energy shortage in future due to the depletion of fossil fuel resources, increased energy demands, and the harmful environmental impacts of current energy resources [1]. Therefore, significant research has been focused on the development of new, efficient, and cleaner energy resources to resolve energy and environmental issues [2–4]. Fuel cells (FCs) could be a very good choice for a variety of applications due to the merits of zero-emission, ease of handling, low operating temperature, and high efficiency [5, 6]. Fuel cells allow the direct conversion of the chemical energy contained in the hydrogen-enriched fuel and an oxidant into electrical energy through electrochemical oxidation with minimum power losses. Among the various types of fuel cells, direct alcohol fuel cells are promising options due to some unique characteristics such as low permeability in the proton exchange membrane (PEM), along with high energy and power densities [7]. However, compared to direct methanol fuels (DMFCs), direct ethanol fuel cells (DEFCs) have been considered a more appealing candidate due to higher energy density, lower toxicity, volatility, and crossover rate [8]. Moreover, ethanol could be produced from a wide variety of renewable sources [9]. Despite these potential advantages, low electrocatalytic activity and the high cost of anode catalyst for ethanol oxidation are of great significance [10]. Accordingly, considerable attention has been devoted to anode catalyst development and structure engineering perspectives to develop the catalyst that possesses high electrocatalytic activity and stability with the merits of low cost. There is no doubt that platinum (Pt) has been considered as an efficient electrocatalyst for ethanol oxidation reaction but the use of platinum is quite limited due to its high cost, the paucity of noble metals, and loss of activity through poisoning by reactive intermediates [11–15]. Hence, to solve these

✉ Zafar Khan Ghouri
zafar_khan.ghouri@qatar.tamu.edu;
zafarkhanghouri@hotmail.com

[1] Chemical Engineering Program, Texas A&M University at Qatar, P.O. 23874, Doha, Qatar

[2] Department of Applied Chemistry & Chemical Technology, University of Karachi, Karachi, Pakistan

problems, various Pt-based bimetallic alloys (PtRu, PtPd, and PtSn) have been used to enhance the catalytic activity and reduce the cost; on the other hand, these Pt-based bimetallic electrocatalysts seriously suffer from heavy aggregation [16–18]. To address this problem, as an alternative to precious metals, to minimize the cost of the metal catalyst, and to reduce the catalyst poisoning, various carbon supports such as graphene [19, 20], multiwall carbon nanotube [21], activated carbon [22], and carbon nanofibers [23] have often been used as supporting materials for both precious and non-precious functional materials. However, as an alternative to the existing commercial activated carbon, a large number of natural sources such as nutshell, coconut shell, peanut, sugarcane bagasse, sawdust, rice husks have been used to synthesize activated carbon [24–29]. In particular, spent coffee ground (SCG) is a suitable raw source for the synthesis of valuable carbonous materials, and it is one of the widely consumed beverages and most popular commodities all around the world. Further, it is grown in more than 80 territories and more than 6 million tons of SCG are produced annually [30]. It is well known that the high surface area and porosity of the carbonous materials are the basic requirements in electrocatalysis. Typically, chemical activation or high-temperature steam activation processes are used to increase the surface area and porosity of the carbonous materials. Chemical activation generally involves two steps: carbonization and activation. Normally, the carbon precursor is soaked with a suitable activating agent such as zinc chloride ($ZnCl_2$), phosphoric acid (H_3PO_4), sulphuric acid (H_2SO_4), potassium hydroxide (KOH), sodium hydroxide (NaOH), and potassium carbonate K_2CO_3 before the carbonization step [31–34]. Zinc chloride has been widely used for chemical activation due to its earth-abundance and unique properties. However, the main objective of this work was to synthesize relatively cheap and effective electrocatalyst from SCG for ethanol electrooxidation. Therefore, the activation of carbon derived from SCG was performed with $ZnCl_2$. Interestingly, $ZnCl_2$ acts as a pore-forming agent as well as a precursor for ZnO. In particular, ZnO-based nanocomposites as a low-cost alternative for noble metals are used in fuel cell applications [35, 36]. Besides the semiconducting and piezoelectric properties, its d-orbital holes are easily valence, which may enhance its catalytic activity [2]. In this work, carbon microbead-encapsulated ZnO particles (CM-ZnO) have been synthesized from SCG by simple approach, involving a chemical activation and subsequent calcination at 700 °C and used as an electrocatalyst for ethanol electrooxidation in the alkaline medium. The introduced CM-ZnO demonstrated distinct textural characteristics that resulted in an enhanced catalytic activity toward ethanol electrooxidation.

2 Experimental

2.1 Materials and preparation of carbon microbead-encapsulated ZnO particles

The following materials were used as received: Spent coffee grounds (SCG) were obtained from a local coffee shop and 98% Zinc Chloride ($ZnCl_2$, Samchun Pure Chemicals, South Korea). All the remaining reagents were used without further purification as they are of the required analytical grade. First, the obtained SCG was dried at 50 ℃ for 6 h. Then a solution of $ZnCl_2$ was prepared by stirring 5.0 g of $ZnCl_2$ in 500 ml deionized water overnight at room temperature. Then 5.0 g of SCG was added and mixed with the $ZnCl_2$ solution and left overnight. The mixture was then filtered and washed six times with deionized water and finally, the produced solid was dried in a vacuum oven at 60 ℃ for 12 h. After drying the mixture, it was calcined in a tubular furnace under the flow of N_2 gas at a temperature of 700 ℃ for 2 h. Figure 1 shows a schematic of the CM-ZnO preparation process.

2.2 Characterization

The crystal structure of the final product was characterized by X-ray diffraction (XRD, Rigaku, Japan with Cu-Kα($\lambda = 1.54056$ A) operating at 45 kV and 100 mA over a range of 2θ angle from 10° to 90°, scanning at a 2θ rate of 4°/min. The morphological characterizations were examined by field-emission scanning electron microscopy (FE-SEM, Hitachi S-7400, Japan) and transmission electron microscopy (TEM, JEOL JEM-2200FS Japan, coupled with rapid energy-dispersive spectroscopy EDAX) operating at 200 kV, while the BET surface areas and pore size distributions were analyzed by physisorption techniques (Micromeritics ASAP 2020 analyzer, USA).

2.3 Preparation of working electrode

Before the fabrication of the working electrode, the apparent electrode area was polished with diamond suspension. Then 2 mg of the as-prepared CM-ZnO was dispersed in 20 µL of Nafion (5 wt %) and 400 µL of isopropanol by ultrasonication for 30 min at room temperature. 15 µL of the formed suspension was then spread by a micro-pipette on to the active area of the glassy carbon electrode, which was then dried at 80 °C for 20 min.

2.4 Electrochemical measurement

The electrochemical measurements were carried out in three-electrode electrochemical cell (VersaSTAT 4, USA)

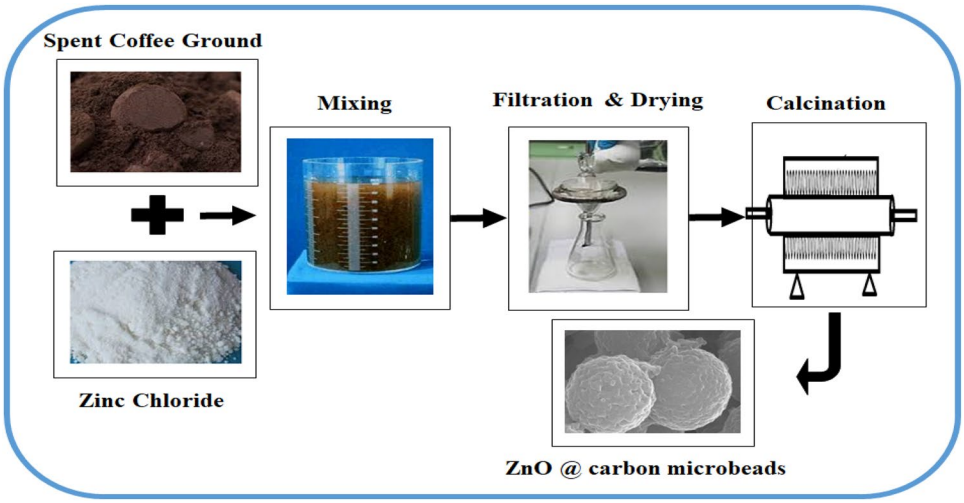

Fig. 1 Schematic diagram for the CM-ZnO preparation process

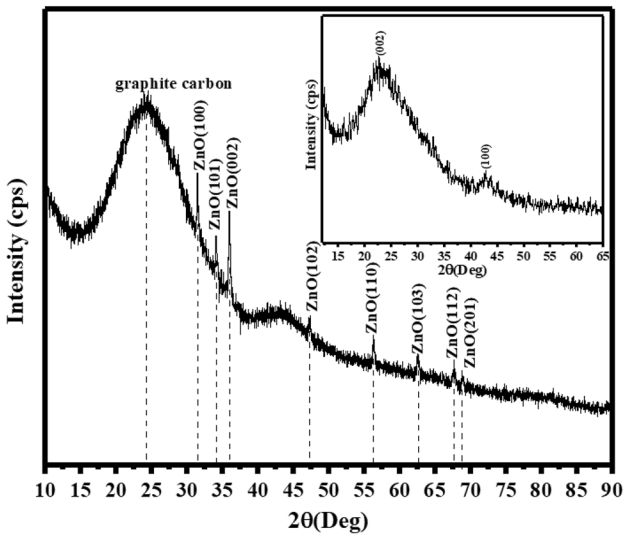

Fig. 2 XRD pattern of the synthesized CM-ZnO particles and inset shows the XRD pattern of non-activated SCG

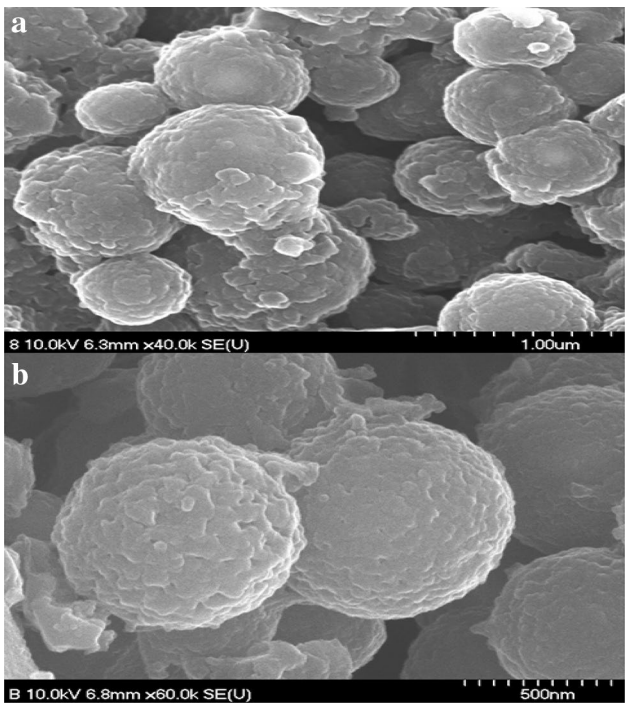

Fig. 3 **a** Low- and **b** high-magnification SEM images of the synthesized CM-ZnO particles

at room temperature. A glassy carbon electrode was used as a working electrode; however, Pt wire and an Ag/AgCl was used as the auxiliary and reference electrodes, respectively.

3 Results and discussion

3.1 Characterization of CM-ZnO

The crystallographic structure of the non-activated carbon and the as-prepared carbon microbead-encapsulated ZnO particles (CM-ZnO) was characterized by XRD, and is shown in Fig. 2. As shown in the inset of Fig. 2, there appear two broad diffraction peaks at 2θ values of ~ 25° and ~ 42° corresponding to (002) and (100) structural phases, respectively, which confirms the existence of graphite crystallite in the non-activated SCG. The as-prepared CM-ZnO particles show similar XRD patterns, shown in the main panel of Fig. 2, with additional sharp diffraction peaks at 2θ values of 31.69°, 34.38°, 36.18°, 47.45°, 56.46°, 62.76°, 67.80°, and 68.92° representing (100), (002), (101), (102), (110), (103), (112), and (201) of hexagonal structure of ZnO, respectively, in accordance with JCPDS card number 01–079–0207. No diffraction peaks for the $ZnCl_2$ precursor are detected, which means that CM-ZnO has high

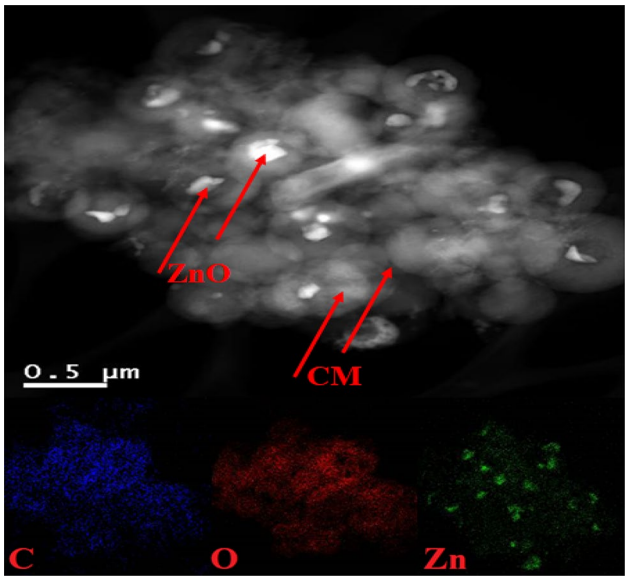

Fig. 4 TEM image and corresponding elemental maps for Zn, O, and C of the synthesized CM-ZnO particles; inset: composition of CM-ZnO particles

Table 1 Composition of CM-ZnO particles obtained by SEM–EDX analysis

Elements	Wt(%)	Atomic (%)
C	86.84	90.58
O	7.66	5.13
Zn	5.5	4.29
Total	100	100

phase purity, with complete calcination of $ZnCl_2$. Figure 3 shows the typical morphology of CM-ZnO, and low-magnification image in Fig. 3a shows that the product consists of a large number of microspheres with a diameter range of about 0.4–0.5 µm, while a high-magnification image, in Fig. 3b, reveals that the surface of the CM-ZnO is rough and entirely spherical in nature. The microspheres' morphology of the as-prepared CM-ZnO was further characterized by TEM and can be clearly noted that numerous ZnO particles are encapsulated inside the carbon microbeads perfectly interconnected together to form the core–shell structure, as shown in Fig. 4. Furthermore, elemental mapping analysis in Fig. 4 reveals the existence and well distribution of carbon, oxygen, and zinc elements; it can be clearly noted that zinc and oxygen counterparts are concentrated in a specific area and revealed that the carbon as a shell is evenly distributed on the surface of ZnO core in the form of carbon microbeads. The elemental composition of CM-ZnO as obtained by EDS analysis is summarized in Table 1, showing 5.5 wt% Zn, 7.66 wt% O, and 86.84 wt% C.

Catalysts' specific surface area is a key factor which directly affects the electrooxidation properties of the catalysts; the higher surface area offers more active sites for catalytic reaction, leading to an improvement in electrooxidation processes. Therefore, the surface area and pore size distribution of the CM-ZnO and non-activated SCG were examined by Brunauer–Emmett–Teller (BET) and Barrett–Joyner–Halenda (BJH) techniques; the results are shown in Fig. 5a–d and the values for the BET specific surface area S_{BET}, pore diameter R_{BJH}, and pore volume V_t are given in Table 2. The characteristic N_2 adsorption–desorption isotherm of non-activated SCG exhibited type IV isotherm and shows a distinct hysteresis loop of N_2, indicating the existence of mesoporous structure (Fig. 5c). Interestingly, the Barrett–Joyner–Halenda (BJH) pore size distribution plot in Fig. 5d declares the existence of a mesoporous structure with wide and irregular distribution of pore diameter. The corresponding BET surface area, pore radius, and pore volume were found to be 6.1 m^2/g, 93.5 Å, and 0.019 cm^3/g, respectively. However, compared with the non-activated SCG, CM-ZnO also displays typical type IV isotherms, as shown in Fig. 5a, with a type H2 hysteresis loop, indicating the existence of mesopores.

On the other hand, the corresponding BJH pore size distribution plot in Fig. 5b confirms the presence of mesopores in the CM-ZnO, with significant increase in the specific surface area and pore volume of the activated sample, which have increased significantly to 210 m^2/g and 1.12 cm^3/g, as can be seen from Table 1, after chemical activation. This could be attributed to the $ZnCl_2$ as an activating agent has introduced defects in the carbon skeleton which led to the increase in porosity. Therefore, the pore volume of the CM-ZnO is higher compared to the non-activated SCG. This, in turn, results in higher surface area. Therefore, it is believed that the mesoporous nature and high surface area of the treated sample provide more active and adsorption sites for electrooxidation.

3.2 Electrochemical measurement

Electrooxidation behavior for evaluating the catalytic activity of the electrodes modified with non-activated SCG and CM-ZnO was performed by cyclic voltammetry (CV) in an electrolyte solution containing ethanol. The corresponding results for 1.0 M KOH and 2.0 M C_2H_5OH + 1.0 M KOH at a scanning rate of 50 mV/s in the potential range from − 0.2 to 1.0 V at room temperature are shown in Fig. 6a and b. Normally, cyclic voltammetry (CV) analysis shows a couple of peaks in anodic and cathode directions, respectively, during the ethanol electrooxidation reaction. These peaks represent the formation of various intermediate products such as CH_3CHO, CH_3COOH, and CO_2 [37]. It can be seen that the electrode modified with non-activated SCG, shown in Fig. 6a, has a very low oxidation performance and delivered low current density of 19 mA/cm^2 at a relatively

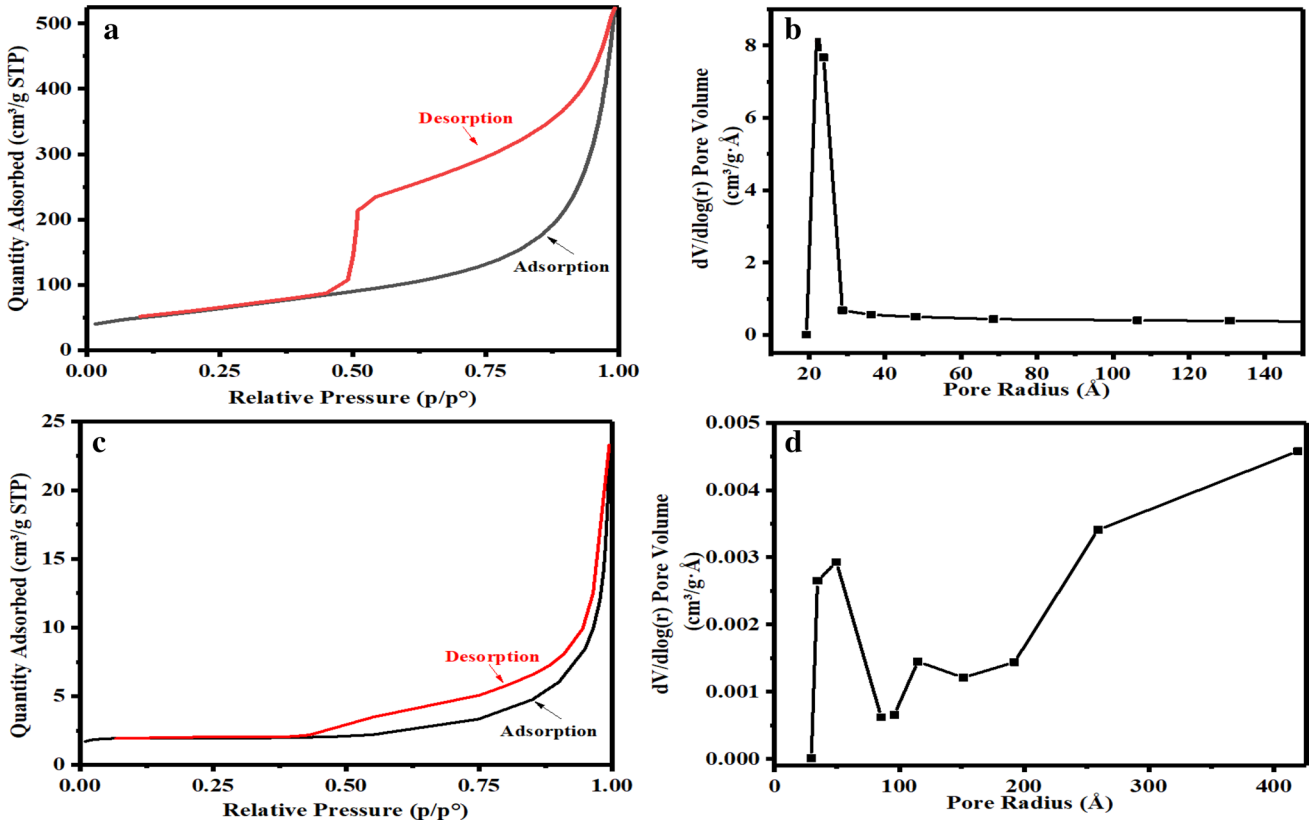

Fig. 5 **a**, **c** N_2 adsorption–desorption isotherm and **b**, **d** corresponding BJH pore size distribution of CM-ZnO particles and non-activated SCG, respectively

Table 2 N_2 adsorption/desorption measurement results of CM-ZnO particles and non-activated SCG

Sample	S_{BET}(m^2/g)	R (Å)	V_t (cm^3/g)
Non-activated SCG	6.1	93.5	0.019
CM-ZnO	212	31.7	1.12

high potential of 0.5 V vs. Ag/AgCl with 2.0 M ethanol; moreover, no characteristic oxidation/reduction peaks were observed. This may be due to the low surface area and absence of ZnO active sites which help in releasing the adsorbed CO-ads, and the oxidation current remains low. On the other hand, a strong influence of the ZnO in CM-ZnO

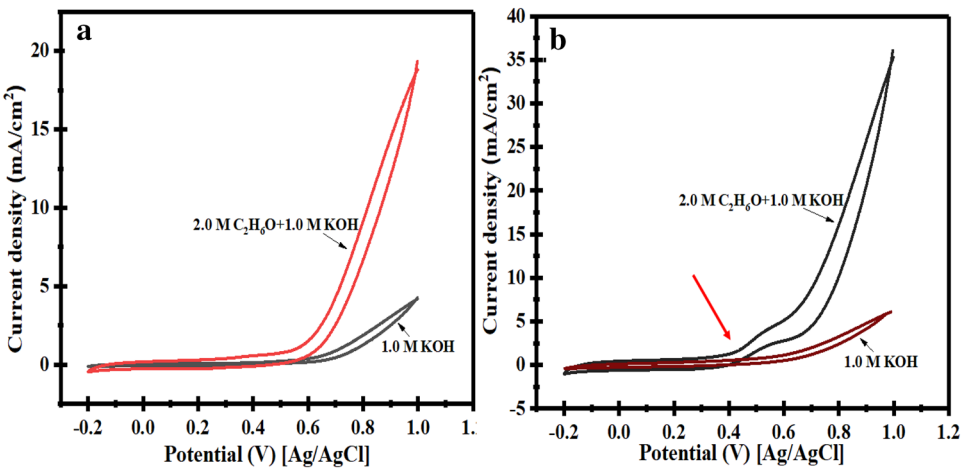

Fig. 6 **a**, **b** CV curve of non-activated SCG and CM-ZnO particles, respectively, in the absence and presence of 2.0 M ethanol in 1.0 M KOH aqueous solution at the scan rate of 50 mV/s

can be observed Fig. 6b. It can be seen, the broad oxidation peaks during the positive scan shows anodic current response and reached to a high current density of 35 mA/cm^2, due to the dehydrogenation of ethanol. After the dissociative adsorption of water, the oxidation of adsorbed species produced acetic acid, which then produces CO_2 on further oxidation steps as follows:

$$CH_3 - CH_2OH + CM - ZnO \rightarrow [CH_3 - CHO]_{ads,CM-Zn} + 2H^+ + 2e^-$$

$$H_2O + CM - ZnO \rightarrow [OH]_{ads,CM-Zn} + H^+ + e^-$$

$$[CH_3 - CHO]_{ads,CM-Zn} + [OH]_{ads,CM-Zn} + CH_3COOH + H^+ + e^-$$

Apart from current density, onset potential is one of the important factors used for evaluating the efficiency of an electrocatalyst. It is a point at which a rise in current density is observed. The lower the onset potential is, the higher is the electrocatalytic activity [38, 39]. However, besides the increase in the current density, a significant decrease in the onset potential (0.4 V vs. Ag/AgCl) was observed (marked by the red arrow). The high catalytic activity may be attributed to the high surface area and low pore diameter of the CM-ZnO, which may allow the surface of the electrode to have more active sites to promote a higher adsorption capacity of ethanol [2, 23]. However, the border reduction peak during the negative scan is ascribed to the renewed oxidation of the ethanol. Normally, a metal-based catalyst requires surface activation by the formation of the MOOH compound by consecutive cyclic voltammetry cycles [40]. Therefore, redox peaks are observed which shows the formation of MOOH. Accordingly, the absence of reduction peaks in 1.0 M KOH (Fig. 6b) shows that the proposed electrocatalyst does not need surface activation. To confirm this finding, a consecutive cyclic voltammetry experiment has been carried out in 1.0 M KOH solution at a scan rate of 50 mV/s. It can be observed from Fig. 7 that no OOH^- formation peaks appear in both positive and negative scans which indicates that the proposed electrocatalyst is independent of the surface activation process.

Generally, higher concentrations of fuel result in improved electrocatalytic activity, but above a certain critical concentration, the performance is deteriorated [41]. Therefore, the concentration of ethanol was varied (0.5 M, 1.0 M, 2.0 M, and 3.0 M) to study the influence of fuel concentration on the obtained current density. As shown in Fig. 8a, the current density is increasing with the increasing ethanol concentration and reaches its maximum value of 35 mA/cm^2 at 2.0 M, and then decreases to about 30 mA/cm^2 for 3.0 M ethanol, which is consistent with many reported electrocatalysts. Chronoamperometry study was carried out

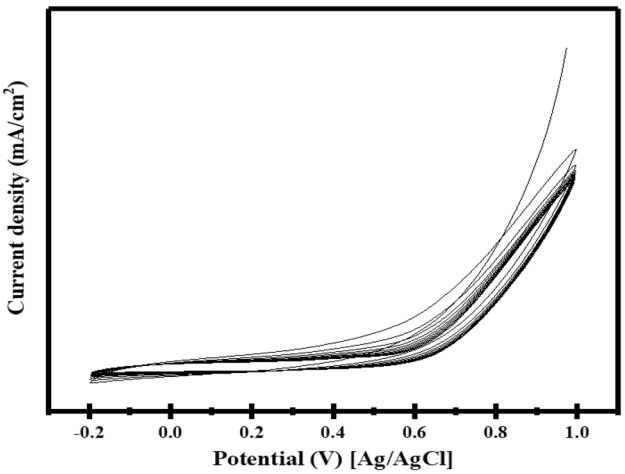

Fig. 7 Consecutive CV curve of CM-ZnO in 1.0 M KOH solution at the scan rate of 50 mV/s

to examine the stability of CM-ZnO particles at a constant potential of 0.4 V vs. Ag/AgCl for 500 s in an alkaline condition of 2.0 M methanol. As shown in Fig. 8b that the current density for ethanol electrooxidation on the proposed electrocatalyst dropped sharply at the beginning due to the formation of intermediate or poisonous species. It is interesting to note that the proposed electrocatalyst get stable just in a few seconds over the entire experiment. Beside the good electrocatalytic activity, the proposed electrocatalyst demonstrates a reasonable stability for the electrooxidation of ethanol.

4 Conclusions

In this work, carbon microbead-encapsulated ZnO particles (CM-ZnO) were successfully synthesized via a very simple and green route from readily available source, spent coffee ground (SCG). Various characterization techniques were utilized to prove that the ZnO particles could be encapsulated within the carbon microbeads. The prepared CM-ZnO particles were found to possess better catalytic properties of higher specific surface area, pore volume, and pore radius within the mesopore range. The electrooxidation behavior of ethanol toward CM-ZnO revealed a reasonable current density of 35 mA/cm^2 at 0.4 V vs. Ag/AgCl. The consecutive CV behavior shows that the introduced CM-ZnO does not require surface activation. Moreover, a significant decrease in the onset potential (0.4 V vs. Ag/AgCl) was observed, which indicates that CM-ZnO particles could be a potential candidate for ethanol oxidation. In future work, it would be motivating to investigate the effects of other activating agents, impregnation time, and calcination temperature on the physicochemical properties of these materials, as well as

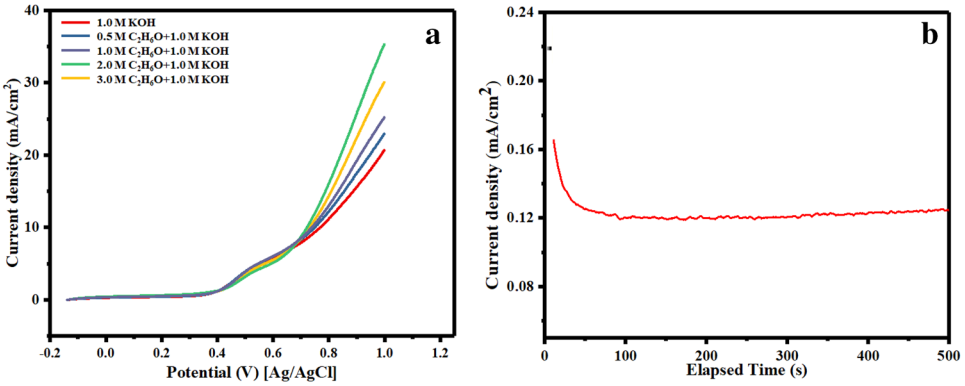

Fig. 8 **a** Influence of ethanol concentration on the electrocatalytic activity of synthesized CM-ZnO particles and **b** chronoamperometry study at $V = 0.4$ V vs./Ag/AgCl in 2.0 M ethanol in alkaline conditions

their potential application for the other energy storage and conversion devices as electrode material.

Acknowledgements Open Access funding provided by the Qatar National Library.

Compliance with ethical standards

Conflict of interest The authors declare no conflict of interest.

References

1. T. Sofien, A. Omri, Literature survey on the relationships between energy variables, environment and economic growth. Renew. Sustain. Energy Rev. **69**, 1129–1146 (2016)
2. Z. Zhang et al., One-pot synthesis of PdZnO/C by microwave sintering method as an efficient electro catalyst for ethanol oxidation reaction. Int. J. Hydrogen Energy **44**(13), 6608–6611 (2019)
3. R. Carrera-Cerritos et al., Performance and stability of Pd nanostructures in an alkaline direct ethanol fuel cell. J. Power Sources **269**, 370–378 (2014)
4. R.C. Cerritos et al., Morphological effect of Pd catalyst on ethanol electro-oxidation reaction. Materials **5**(9), 1686–1697 (2012)
5. Y. Hu et al., Effects of structure, composition, and carbon support properties on the electrocatalytic activity of Pt-Ni-graphene nanocatalysts for the methanol oxidation. Appl. Catal. B **111**, 208–217 (2012)
6. C.H.A. Tsang, D. Leung, Use of Pd-Pt loaded graphene aerogel on nickel foam in direct ethanol fuel cell. Solid State Sci. **75**, 21–26 (2018)
7. S. Zhang et al., Tuning the electronic structure of platinum nanocrystals towards high efficient ethanol oxidation. Chin. J. Catal. **40**(12), 1904–1911 (2019)
8. L. An, T.S. Zhao, Y.S. Li, Carbon-neutral sustainable energy technology: direct ethanol fuel cells. Renew. Sustain. Energy Rev. **50**, 1462–1468 (2015)
9. M.Z. Yazdan-Abad et al., Pd nanonetwork decorated on rGO as a high-performance electrocatalyst for ethanol oxidation. Appl. Surf. Sci. **462**, 112–117 (2018)
10. J. Wang et al., MoS2 nanoflower supported Pt nanoparticle as an efficient electrocatalyst for ethanol oxidation reaction. Int. J. Hydrogen Energy **44**(31), 16411–16423 (2019)
11. L.T. Tran et al., Preparation and electrocatalytic characteristics of the Pt-based anode catalysts for ethanol oxidation in acid and alkaline media. Int. J. Hydrogen Energy **43**(45), 20563–20572 (2018)
12. T. Iwasita et al., Progress in the study of electrocatalytic reactions of organic species. Electrochim. Acta **39**(11–12), 1817–1823 (1994)
13. F. Delime, J. Leger, C. Lamy, Enhancement of the electrooxidation of ethanol on a Pt–PEM electrode modified by tin. Part I: Half cell study. J. Appl. Electrochem. **29**(11), 1249–1254 (1999)
14. F. Vigier et al., On the mechanism of ethanol electro-oxidation on Pt and PtSn catalysts: electrochemical and in situ IR reflectance spectroscopy studies. J. Electroanal. Chem. **563**(1), 81–89 (2004)
15. C. Xu, P. Kang Shen, Y. Liu, Ethanol electrooxidation on Pt/C and Pd/C catalysts promoted with oxide. J. Power Sources **164**(2), 527–531 (2007)
16. A. Hajian et al., Nanostructured flower like Pt-Ru for ethanol oxidation and determination. J. Electrochem. Soc. **162**(1), B41–B46 (2015)
17. H. Zhang et al., Facile synthesis of Pd–Pt alloy nanocages and their enhanced performance for preferential oxidation of CO in excess hydrogen. ACS Nano **5**(10), 8212–8222 (2011)
18. M. Nakamura et al., Ethanol oxidation on well-ordered PtSn surface alloy on Pt (111) electrode. J. Phys. Chem. C **117**(35), 18139–18143 (2013)
19. N.A. Barakat et al., Nickel nanoparticles-decorated graphene as highly effective and stable electrocatalyst for urea electrooxidation. J. Mol. Catal. A **421**, 83–91 (2016)
20. Y. Shen et al., Comparison study of few-layered graphene supported platinum and platinum alloys for methanol and ethanol electro-oxidation. J. Power Sources **278**, 235–244 (2015)
21. L.Q. Hoa et al., Functionalized multi-walled carbon nanotubes as supporting matrix for enhanced ethanol oxidation on Pt-based catalysts. Electrochem. Commun. **13**(7), 746–749 (2011)

22. E.L. da Silva et al., Influence of activated carbon porous texture on catalyst activity for ethanol electro-oxidation. Int. J. Hydrogen Energy **39**(27), 14760–14767 (2014)
23. Y.-H. Qin et al., Effect of carbon nanofibers microstructure on electrocatalytic activities of Pd electrocatalysts for ethanol oxidation in alkaline medium. Int. J. Hydrogen Energy **35**(15), 7667–7674 (2010)
24. A. Ahmadpour, D. Do, The preparation of activated carbon from macadamia nutshell by chemical activation. Carbon **35**(12), 1723–1732 (1997)
25. C.J. Kirubakaran, K. Krishnaiah, S. Seshadri, Experimental study of the production of activated carbon from coconut shells in a fluidized bed reactor. Ind. Eng. Chem. Res. **30**(11), 2411–2416 (1991)
26. K. Periasamy, C. Namasivayam, Removal of copper (II) by adsorption onto peanut hull carbon from water and copper plating industry wastewater. Chemosphere **32**(4), 769–789 (1996)
27. K. Cronje et al., Optimization of chromium (VI) sorption potential using developed activated carbon from sugarcane bagasse with chemical activation by zinc chloride. Desalination **275**(1–3), 276–284 (2011)
28. K. Mohanty, D. Das, M. Biswas, Adsorption of phenol from aqueous solutions using activated carbons prepared from Tectona grandis sawdust by $ZnCl_2$ activation. Chem. Eng. J. **115**(1–2), 121–131 (2005)
29. J. Sahu et al., Performance of a modified multi-stage bubble column reactor for lead (II) and biological oxygen demand removal from wastewater using activated rice husk. J. Hazard. Mater. **161**(1), 317–324 (2009)
30. L. Zhang, X. Sun, Using cow dung and spent coffee grounds to enhance the two-stage co-composting of green waste. Bioresour. Technol. **245**, 152–161 (2017)
31. V. Fierro, V. Torné-Fernández, A. Celzard, Kraft lignin as a precursor for microporous activated carbons prepared by impregnation with ortho-phosphoric acid: synthesis and textural characterisation. Microporous Mesoporous Mater. **92**(1–3), 243–250 (2006)
32. J.I. Hayashi et al., Preparing activated carbon from various nutshells by chemical activation with K2CO3. Carbon **40**(13), 2381–2386 (2002)
33. C. Singh et al., Studies on the removal of Pb (II) from wastewater by activated carbon developed from Tamarind wood activated with sulphuric acid. J. Hazard. Mater. **153**(1–2), 221–228 (2008)
34. J. Acharya et al., Removal of lead (II) from wastewater by activated carbon developed from Tamarind wood by zinc chloride activation. Chem. Eng. J. **149**(1–3), 249–262 (2009)
35. Z.K. Ghouri et al., Nano-engineered ZnO/CeO_2 dots@CNFs for fuel cell application. Arab. J. Chem. **9**(2), 219–228 (2016)
36. G.M.K. Tolba et al., Hierarchical TiO_2/ZnO nanostructure as novel non-precious electrocatalyst for ethanol electrooxidation. J. Mater. Sci. Technol. **31**(1), 97–105 (2015)
37. J. Zhang, *PEM Fuel Cell Electrocatalysts and Catalyst Layers: Fundamentals and Applications* (Springer Science & Business Media, London, 2008)
38. A.N. Vyas, G.D. Saratale, S.D. Sartale, Recent developments in nickel based electrocatalysts for ethanol electrooxidation. Int. J. Hydrogen Energy **45**(10), 5928–5947 (2019)
39. Z.K. Ghouri et al., Applicable anode based on Co_3O_4–$SrCO_3$ heterostructure nanorods-incorporated CNFs with low-onset potential for DUFCs. Appl. Nanosci. **7**(8), 625–631 (2017)
40. N.A. Barakat et al., Distinct influence for carbon nano-morphology on the activity and optimum metal loading of Ni/C composite used for ethanol oxidation. Electrochim. Acta **182**, 143–155 (2015)
41. Z.K. Ghouri et al., Influence of copper content on the electrocatalytic activity toward methanol oxidation of CoχCuy alloy nanoparticles-decorated CNFs. Sci. Rep. **5**, 16695 (2015)